JACC: BASIC TO TRANSLATIONAL SCIENCE VOL. 5, NO. 12, 2020

PRECLINICAL RESEARCH

Absence of NLRP3 Inflammasome in Hematopoietic Cells Reduces Adverse Remodeling After Experimental Myocardial Infarction

Mieke C. Louwe, PhD,[a] Maria B. Olsen, PhD,[a,*] Ole J. Kaasbøll, MD, PhD,[b,*] Kuan Yang, MSc,[a] Linn E. Fosshaug, MD, PhD,[a,c] Katrine Alfsnes, MSc,[a] Jonas D.S. Øgaard, BSc,[a] Azita Rashidi, BSc,[a] Vidar M. Skulberg, Cand Mag,[d] Mingyi Yang, PhD,[e] Davi de Miranda Fonseca, PhD,[f] Animesh Sharma, PhD,[f] Jan Magnus Aronsen, MD, PhD,[d,g] Elisabeth Schrumpf, MD, PhD,[a,c,h] Muhammad Shakil Ahmed, PhD,[b] Christen Peder Dahl, MD, PhD,[a] Tuula A. Nyman, PhD,[i] Thor Ueland, PhD,[a,c] Espen Melum, MD, PhD,[a,c,h,j] Bente E. Halvorsen, PhD,[a,c] Magnar Bjørås, PhD,[c,e,k] Håvard Attramadal, MD, PhD,[b,c] Ivar Sjaastad, MD, PhD,[c,d] Pål Aukrust, MD, PhD,[a,c,l] Arne Yndestad, PhD[c]

VISUAL ABSTRACT

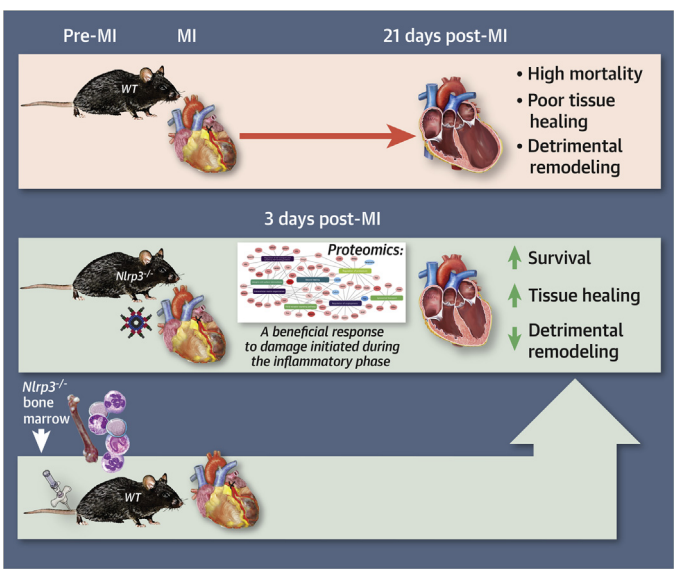

Louwe, M.C. et al. J Am Coll Cardiol Basic Trans Science. 2020;5(12):1210–24.

HIGHLIGHTS

- **NLRP3-deficient mice had improved survival and infarction healing following MI.**
- **Proteomics of infarcted tissue indicated that the beneficial effect of NLRP3 deficiency manifests during the early inflammatory phase, resulting in a more favorable tissue repair response.**
- **The beneficial phenotype was recapitulated in wild-type mice receiving bone marrow from *Nlrp3*$^{-/-}$ mice.**

From the [a]Research Institute of Internal Medicine, Oslo University Hospital, Oslo, Norway; [b]Institute for Surgical Research, Oslo University Hospital, Oslo, Norway; [c]Faculty of Medicine, University of Oslo, Oslo, Norway; [d]Institute for Experimental Medical Research, Oslo University Hospital Ullevål, Oslo, Norway; [e]Department of Microbiology, Oslo University Hospital Rikshospitalet, Oslo, Norway; [f]PROMEC Core Facility for Proteomics and Metabolomics, Norwegian University of Science and Technology, Trondheim, Norway; [g]Bjørknes College, Oslo, Norway; [h]Norwegian PSC Research Center, Department of Transplantation Medicine, Division of Surgery, Inflammatory Diseases and Transplantation, Oslo University Hospital Rikshospitalet, Oslo, Norway; [i]Department of Immunology, Institute of Clinical Medicine, University of Oslo and Rikshospitalet Oslo, Oslo, Norway; [j]Section for Gastroenterology, Department of Transplantation Medicine, Division of Surgery, Inflammatory Diseases and Transplantation, Oslo University Hospital Rikshospitalet, Oslo, Norway; [k]Department of Clinical and Molecular Medicine, Norwegian University of

ISSN 2452-302X https://doi.org/10.1016/j.jacbts.2020.09.013

SUMMARY

An inflammatory response is required for tissue healing after a myocardial infarction (MI), but the process must be balanced to prevent maladaptive remodeling. This study shows that improved survival and cardiac function following MI, in mice deficient for the NLRP3 inflammasome, can be recapitulated in wild-type mice receiving bone marrow from *Nlrp3*$^{-/-}$ mice. This suggests that NLRP3 activation in hematopoietic cells infiltrating in the myocardium increases mortality and late ventricular remodeling. Our data should encourage performing clinical trials directly targeting NLRP3 inflammasome and their inflammatory cytokines (interleukin-1β and -18) in MI patients. (J Am Coll Cardiol Basic Trans Science 2020;5:1210–24)

ABBREVIATIONS AND ACRONYMS

ASC = apoptosis-associated speck like protein

CMR = cardiac magnetic resonance

ECM = extracellular matrix

HF = heart failure

IL = interleukin

I/R = ischemia/reperfusion

LV = left ventricle/ventricular

MI = myocardial infarction

NLRP3 = NLR family, pyrin domain containing protein 3

WT = wild-type

Myocardial infarction (MI) induces a sterile inflammatory response that is a prerequisite for tissue healing. However, excessive or prolonged inflammation may also result in infarct expansion and adverse left ventricular (LV) remodeling, leading to impaired myocardial function and heart failure (HF) (1). Emerging evidence suggests that the myocardial response to MI is regulated by innate immune receptors, which are likely to be important in this process (2,3).

NLRP3 (NLR family, pyrin domain containing protein 3) is a cytosolic innate immune receptor that, upon activation, forms a multiprotein complex named NLRP3 inflammasome, together with the adaptor protein apoptosis-associated speck like protein (ASC) and caspase-1 (4). Active caspase-1 cleaves the pre-formed pro-interleukin (IL)-1β and IL-18 to their active and secreted forms. IL-1β and -18 are potent up-stream inflammatory cytokines, which initiate a cascade of inflammatory events including leukocyte recruitment and activation to the site of inflammation (5).

Although the role of the NLRP3 inflammasome in atherosclerosis is established (6), its role during MI and the following myocardial remodeling is still unclear. In mice, somewhat conflicting results have been reported in relation to the role of ASC and NLRP3 in ischemia/reperfusion (I/R) injury, at least partly depending on the experimental models (7–10). Moreover, data from ASC and caspase-1-deficient mice may not necessarily reflect the effects of the NLRP3 inflammasome alone, as these molecules are also components of other inflammasomes (4). Mezzaroma et al. (11) investigated the effect of siRNA knockdown of NLRP3 up to 7 days after MI, which prevented inflammasome formation, and this resulted in improved function and reduced cardiac enlargement. More recently, van Hout et al. (12) showed that NLRP3 inflammasome inhibition reduced infarct size and preserved cardiac function in transluminal balloon occluded female pigs during 7-day follow-up. However, due to the difference in infarct size that most studies have been focusing on, all observed effects on cardiac function and remodeling could be secondary to this, and the role of the NLRP3 inflammasome in these processes following MI is still unclear. Moreover, data on the effect of NLRP3 deficiency on myocardial remodeling following MI after the first week are scarce.

To further elucidate the role of NLRP3 inflammasome during MI, we examined short-term (7 days) and long-term (21 days) effects of MI on survival and myocardial remodeling in wild-type (WT) and *Nlrp3*$^{-/-}$ mice. To examine phenotypes that were not purely dependent on infarct size and I/R injury, we used a model of permanent ligation. Our experimental data shows decreased mortality during the first week in *Nlrp3*$^{-/-}$ mice. Furthermore, cardiac remodeling was less detrimental in *Nlrp3*$^{-/-}$ mice up to 21 days post-MI, with no differences in infarct size between the 2 genotypes. Finally, the importance of immune cells for the beneficial phenotype of *Nlrp3*$^{-/-}$ mice was demonstrated by the recapitulation of the

Science and Technology, Trondheim, Norway; and the [l]Section of Clinical Immunology and Infectious Diseases, Oslo University Hospital Rikshospitalet, Oslo, Norway. *Drs. Olsen and Kaasbøll contributed equally to this work.

The authors attest they are in compliance with human studies committees and animal welfare regulations of the authors' institutions and Food and Drug Administration guidelines, including patient consent where appropriate. For more information, visit the Author Center.

Manuscript received December 18, 2019; revised manuscript received September 22, 2020, accepted September 22, 2020.

Nlrp3$^{-/-}$ phenotype in WT mice that had been transplanted with *Nlrp3*$^{-/-}$ bone marrow.

METHODS

MICE. C57BL/6J mice, used as WT control, and *Nlrp3*$^{-/-}$ mice, generated as previously described (13,14) and backcrossed at least 7 times on a C57BL/6J genetic background, were age matched for all experiments. Mice were bred and housed under standard conditions with *ad libitum* access to food and water at the Centre for Comparative Medicine, Oslo University Hospital.

In all parts of the study, the investigators were blinded in relation to the genotypes.

MOUSE MODEL OF EXPERIMENTAL MI. MI surgery was performed as previously described (15). Briefly, mice were anesthetized with a mixture of O_2 and 3% isoflurane, the heart was exteriorized through a left thoracotomy at the fifth intercostal space, and the left coronary artery was ligated 2 to 3 mm from its proximal origin inducing an MI. Following ligature placement, the heart was immediately positioned back in the thoracic cavity, followed by evacuation of pneumothorax and wound closure. Buprenorphine (Temgesic; 0.1 mg/kg, Indivior, North Chesterfield, Virginia) was administered subcutaneously prior to recovery from anesthesia. All animals, except the bone marrow transplantation mice, were 8-10 weeks at the time of surgery.

BONE MARROW TRANSPLANTATION. WT and *Nlrp3*$^{-/-}$ male mice on a C57BL/6J background, expressing the CD45.2 allele, and B6.SJL-Ptprca Pepcb/BoyJ male mice, expressing the CD45.1 allele, were used to generate mice that specifically lack either WT or NLRP3 in bone marrow-derived cells. WT and B6.SJL-Ptprca Pepcb/BoyJ male mice were exposed to 2 dosages of 6 Gy (0.76 Gy/min, 300 kV, 10 mA) total body irradiation with 4 h in between, using an Xstrahl research cabinet Rontgen source. Bone marrow was isolated from B6.SJL-Ptprca Pepcb/BoyJ and *Nlrp3*$^{-/-}$ mice by flushing femurs and tibias with phosphate-buffered saline (PBS). Single-cell suspensions were prepared by passing the cells through a 40-μm nylon cell strainer. Irradiated recipient WT and B6.SJL-Ptprca Pepcb/BoyJ mice received 1×10^6 bone marrow cells from B6.SJL-Ptprca Pepcb/BoyJ and *Nlrp3*$^{-/-}$ mice, respectively, by intravenous injection into the tail vein. Engraftment of bone marrow was confirmed after 8 weeks of recovery by flow cytometry in whole blood samples, as indicated by expression of CD45.1 or CD45.2 (Supplemental Figure S1). Nine weeks after bone marrow transplantation, an MI was induced. The age of the animals were then approximately 17 weeks.

MORTALITY STUDIES. During the 3 mortality studies, mice were checked at least once a day by a researcher, in addition to routine checks by the animal caretakers. Mice showing signs of suffering were scored according to predefined criteria including, but not limited to, 15% bodyweight reduction, reduced locomotor activity, and reduced behavioral activity, and were euthanized if not reverting to a score above the cutoff value for humane endpoints within 1 h after a repeated administration of buprenorphine (0.1 mg/kg). Both mice that died and mice that were euthanized due to humane endpoints were registered as mortalities. All mice that died or were euthanized were autopsied by an abdominal skin incision right below the rib-cage, followed by inspection of the thoracic cavity and then an incision of the diaphragm along the rib cage. Large amount of blood clots around the heart and in the thorax cavity counted as rupture. In most cases, rupture site in the heart was also located for these animals. No signs of rupture, confirmed infarction, and lung edema were considered as acute heart failure. All researchers were blinded for the genotypes.

CARDIAC MAGNETIC RESONANCE. Cardiac magnetic resonance (CMR) experiments were performed using a 9.4-T preclinical magnetic resonance system (Agilent Technologies, Inc., Palo Alto, California) with high-performance gradient insert (60 mm ID, rise time 180 μs, max strength 100 gauss/cm) and quadrature volume RF coils (35 mm ID, Rapid Biomedical GmbH, Rimpar, Germany) dedicated to mouse imaging. Anesthesia was induced in a chamber with a mixture of O_2 and 4% isoflurane, and was further maintained by administration of a mixture of O_2 and 1.5% to 2% isoflurane in freely breathing mice. Temperature was maintained around 37°C by heated air. Cardiac and respiratory gated cine-CMR was acquired in the true short-axis orientation. The key parameters were 1-mm slice thickness; TE/TR 2.2/4.6 ms; 2 averages; field of view 25.6 × 25.6 mm; matrix size 128 × 128; and flip angle 15°. CMR data was analyzed using Fiji (ImageJ) software (16) with the operator blinded to animal groups.

ECHOCARDIOGRAPHY. Echocardiography was performed under standardized conditions with the mice in a supine position, spontaneously breathing 1.5% isoflurane mixed with 98.5% O_2 via a mask. Standard parasternal long- and short-axis images were acquired with the Vevo 2100 system and analyzed offline using Vevo 2100 1.4.1 software (VisualSonics, Toronto, Ontario, Canada). Three consecutive

M-mode long-axis cardiac cycles were analyzed and averaged.

BLOOD AND TISSUE SAMPLING. Mice were anaesthetized with 4% isoflurane supplemented with O_2. The right carotid artery was exposed and incised and arterial blood was collected together with 50 μl of 0.5 mol ethylenediaminetetraacetic acid. Plasma was prepared by centrifugation at 2,000 *g* for 20 min at 4°C, snap-frozen in liquid N_2, and stored at −80°C.

Hearts were collected, separated into LV and RV, rinsed in PBS, blotted dry, and weighted. A standardized 2-mm slice from the LV, using a mouse heart slicer matrix (Zivic instruments, Pittsburgh, Pennsylvania), was collected for histology and fixated in 4% formaldehyde (Histolab Products AB, Gothenburg, Sweden) until further processing. Remaining LV tissue was separated into noninfarcted and infarcted area. Right ventricle, noninfarcted, and infarcted tissue was snap-frozen in liquid N_2 and stored at −80 °C.

mRNA ISOLATION AND REAL-TIME QUANTITATIVE POLYMERASE CHAIN REACTION. Total RNA from mouse LV was extracted using TRIzol (Invitrogen, San Diego, California), DNase treated, cleaned up using RNeasy Mini Columns (Qiagen, Hilden, Germany), and stored at −80°C. cDNA was synthesized from 2 μg RNA using the High Capacity cDNA Reverse Transcription Kit (Thermo Fisher Scientific, Waltham, Massachusetts). Quantification of gene expression was performed in duplicate by quantitative real-time polymerase chain reaction (PCR), using Power Sybr Green Master Mix (Applied Biosystems, Foster city, California) and sequence specific PCR-primers (can be provided upon request).

HISTOLOGY AND IMMUNOHISTOCHEMISTRY. Formalin-fixed hearts were dehydrated, flat embedded in paraffin, and sliced into 5-μm-thick cross-sections. Sections were deparaffinized in xylene and rehydrated in EtOH (4× 100%, 2× 96%, 1× 80%, and 1× 50%).

For immunohistochemical staining, antigen retrieval was obtained boiling for 20 min at 98°C in citrate buffer (pH 6), followed by cooling for 20 min at room temperature (RT). Unspecific binding was blocked using Rodent Block M (Biocare Medical, Concord, San Francisco, California) followed by 1 h incubation with primary antibodies anti-Ly6G 1:750 (127602, Biolegend, London, United Kingdom), anti-Mac2 1:1,500 (CL8942AP, Cedarlane, Burlington, Canada) at RT. After washing, the slides were incubated for 30 min at RT with peroxidase-conjugated secondary antibody (Impress-Vector, Vector Laboratories, Burlingame, California), rinsed, developed with chromogen for immunoperoxidase staining (DAB Plus, Vector Laboratories) and counterstained with hematoxylin. The stained sections were scanned (AxioScan, Carl Zeiss, Oberkochen, Germany) and uploaded to z9.nird.sigma2.no, an in-house made application for evaluation and quantitative examination of histological sections.

Picrosirius red staining for collagen was performed by 1-h incubation in Sirius Red Solution (Histolab Products AB, Gothenburg, Sweden), followed by 2× rinsing steps acidified water with 5% acetic acid. After 2 quick dips in 100% EtOH, sections were rinsed in xylene and mounted with Eukitt (Flyka, Sigma-Aldrich). The stained sections were scanned and uploaded to z9. After exclusion of large blood vessel areas, the level of fibrosis was estimated. Areal positive staining for collagen was quantified relative to total tissue area, based on colorimetric thresholding of the picrosirius red staining in the LAB color space.

For wheat germ agglutinin (WGA) staining, deparaffinization and rehydration was performed as described in the previous text. Sections were boiled at 98°C in citrate buffer (pH 6), followed by 20 min cooling at RT, before overnight incubation at 4°C with Alexa-488 conjugated WGA (1:200, Life Technologies, ThermoFisher Scientific, Waltham, Massachusetts). Sections were rinsed in PBS, mounted with slow fade Gold Antifade Mountant with DAPI (Life Technologies, ThermoFisher Scientific), and scanned and imported into z9. Areas showing cardiomyocyte cross sections were chosen for analyses. Cardiomyocyte area was quantified by an in-house made macro for Fiji (ImageJ).

ANALYSIS OF CYTOKINES. IL-18 was measured by enzyme-linked immunosorbent assay (R and D Systems, Minneapolis, Minnesota), according to manufacturer's protocol.

PROTEOMIC ANALYSIS WITH STABLE ISOTOPE LABELLING BY AMINO ACIDS IN CELLS. Quantitative proteomics with the stable isotope labeling with amino acids in cell culture (SILAC) spike in approach was performed (17). The data were collected from infarcted tissue of WT and *Nlrp3*$^{-/-}$ mice 3 and 5 days post-MI (day 3; n = 6 for WT, n = 5 for *Nlrp3*$^{-/-}$, day 5; n = 3 for WT, n = 4 for *Nlrp3*$^{-/-}$). Differences in protein levels between WT and *Nlrp3*$^{-/-}$ natural (light) isotope $^{12}C_6$-lysine hearts were identified by comparing these with a SILAC $^{13}C_6$-lysine (heavy) reference heart. After data normalization, principal

component analysis was performed for all samples. In the principal component analysis plots, tissue from mice with high lung weights, most likely due to heart failure, appeared as outliers. Due to low number of "high lung weight animals," only mice with normal or moderate lung weight increase were selected for forward statistical analysis, in triplicate for each group. This analysis for protein expression fold changes was performed using R software (R Foundation, Vienna, Austria) and based on the report by Kammers et al. (18). The moderated q and q values were calculated using moderated test statistics of approach Linear Models for Microarray Data (19). The proteins were defined as significant differentially expressed by moderated q value <0.05 and $\log_2$Foldchange ≥2. Metascape (version 3.5) (20) was used to perform the enrichment analysis based on the GeneOntology (21,22), Reactome (23), and KEGG (24–26) databases. The enrichment analysis dot plot was made by ggplot2 R package (27), and the network plot was created using Cytoscape (28).

MACROPHAGE LABEL-FREE QUANTITATIVE PROTEOME ANALYSIS. Peritoneal macrophages from male WT and *Nlrp3*$^{-/-}$ mice were isolated by flushing the peritoneal cavity with 5 ml ice cold serum-free RPMI-1640 (Gibco, ThermoFisher Scientific, 12633). The aspirated fluid was stored on ice until further processing. After centrifugation (300 *g*, 4°C, 7 min), cells were resuspended in serum-free RPMI and seeded in 6-well plates, then incubated for 15 min at RT followed by 1 h at 37°C with 5% CO_2 to allow adhesion. Subsequently, nonadherent cells were washed away with PBS. Remaining cells were lysed in T-PER tissue protein extraction reagent (ThermoFisher Scientific) and proteinase inhibitors were added (Halt Protease Inhibitor Cocktail, ethylenediaminetetraacetic acid-free [100×, ThermoFisher Scientific]). The lysates were spun down (20,000 *g*, 4°C, 10 min) and resuspended in T-PER solution, and protein concentrations were measured with the Pierce BCA Protein Assay kit (Thermo Fisher Scientific). Protein extracts were stored at −80°C until further processing.

For proteomics analysis, the proteins were precipitated with TCA/acetone in −20°C overnight. The precipitated proteins were dissolved with 6 mol urea in 100 mmol/l ammonium bicarbonate, reduced with DTT, and alkylated with iodoacetamide followed by digestion with trypsin overnight in 37°C. The resulting peptides were desalted and concentrated before mass spectrometry by the STAGE-TIP method using a C18 resin disk (3 mol Empore). Each peptide mixture was analyzed by an nEASY-LC coupled to QExactive Plus (ThermoElectron, Bremen, Germany) with EASY Spray PepMap RSLC column (C18, 2 μl, 100Å, 75 μm × 50 cm) using 120-min LC separation gradient. The resulting MS raw files were submitted to the MaxQuant (29) software version 1.6.1.0 for protein identification and label free quantification. The Uniprot database with "mouse" entries (January 2019) was used for the database searches. Perseus (30) software was used for the statistical analysis of the results. Proteins with permutation based false discovery rate (FDR) <0.05 and $\log_2$Foldchange ≥1 were considered as expressed significantly different. Volcano plot was created by Enhanced Volcano R package (31). Enrichment analysis and making of enrichment dot plot were performed as described previously.

EFFEROCYTOSIS ASSAY. Peritoneal lavage was performed as described at the macrophage proteomics paragraph. After centrifugation and resuspension, 60,000 cells were seeded in quadruplets into 96-well flat clear-bottom black-walled polystyrene tissue-culture treated microplates (Corning, Glendale, Arizona) and incubated for 15 min at RT followed by 75 min at 37°C with 5% CO_2 to allow for adhesion. Next, nonadherent cells were washed away with PBS. Prior to efferocytosis experiments, Jurkat T cells were treated with 0.1 μmol/l camptothecin (Sigma-Aldrich) for 16 h to induce apoptosis (>80% annexin A5+ and <10% Viobility+) (Supplemental Figure S2). Subsequently, apoptotic cells were labelled with 80 ng/mL pHrodo Red, succinimidyl ester (Invitrogen, cat P36600) per 10^6 cells for 30 min at RT, hidden from light, washed twice with PBS, and resuspended in RPMI. Next, 90,000 apoptotic Jurkat T cells were added per well (3:2 ratio, Jurkat T cells to macrophages) to peritoneal macrophages in RPMI. The efferocytic capacity of peritoneal macrophages was determined by using overlays of phase contrast and fluorescence images of cells for 2 h incubation in an IncuCyte ZOOM live-cell imaging and analysis platform (Essen BioScience).

STATISTICAL ANALYSIS. GraphPad Prism version 7.0 (GraphPad Software, La Jolla, California) was used for data analysis. Significance of difference between the groups was tested by unpaired, 2-tailed Student's *t*-tests. Survival was assessed using Kaplan-Meier analysis with the log-rank test. Values are presented as mean ± SEM. All p values <0.05 were considered statistically significant.

STUDY APPROVAL. The experimental animal protocols (FOTS id 5926 and 6895) were reviewed and

FIGURE 1 Reduced Mortality in *Nlrp3*$^{-/-}$ Mice Following MI

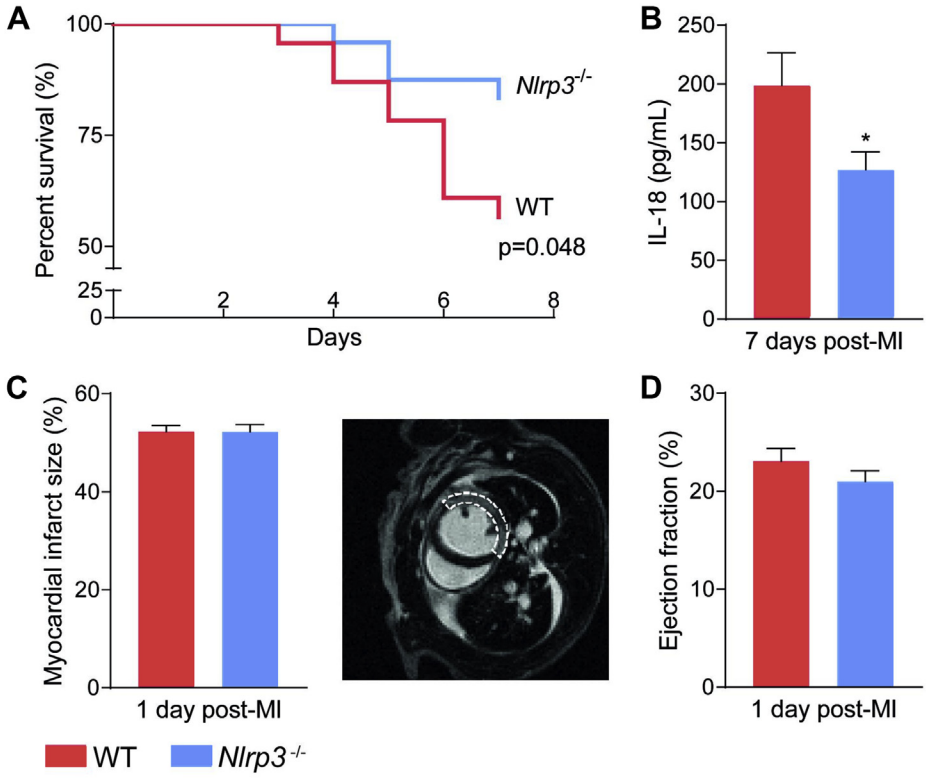

(A) Mortality rates in wild-type (WT) (n = 23) and *Nlrp3*$^{-/-}$ (n = 24) male mice up to 7 days post-myocardial infarction (MI) (p = 0.048, by Kaplan-Meier analysis with log-rank test, 2 independent experiments combined). **(B)** Interleukin (IL)-18 levels in plasma measured by enzyme-linked immunosorbent assay 7 days post-MI (n = 9 mice per genotype). *p<0.05. **(C and D)** Left ventricle infarct size (representative image is shown, **dashed line** shows MI area) and ejection fraction measured 1 day post-MI by CMR (n = 17 mice per genotype). Values are presented as mean ± SEM.

approved by the Norwegian Animal Research Committee and conform to the Guide for the Care and Use of Laboratory Animals published by the U.S. National Institutes of Health (NIH Publication, 8th Edition, 2011).

RESULTS

MORTALITY IN THE SUBACUTE PHASE FOLLOWING MI IS REDUCED IN *NLRP3*$^{-/-}$ MICE. WT and *Nlrp3*$^{-/-}$ mice were subjected to MI by permanent ligation of the left coronary artery and followed for 7 days. WT mice had a higher mortality rate compared with *Nlrp3*$^{-/-}$ mice (43% vs. 17%, respectively; $p < 0.05$) (Figure 1A). The majority of mice died between days 4 and 6, and necropsy showed that irrespective of genotype, the main cause of death was myocardial rupture (8 of 10 WT; 3 of 4 *Nlrp3*$^{-/-}$; the remaining 3 mice reached humane endpoints: they had a reduced body weight of more than 15% and/or showed signs of severe inactivity). The improved survival rate in *Nlrp3*$^{-/-}$ mice was accompanied by significantly lower IL-18 plasma levels, as a marker of NLRP3 activity, 7 days after MI compared with WT mice (–36%; $p < 0.05$) (Figure 1B).

COMPARABLE INFARCT SIZE IN *NLRP3*$^{-/-}$ AND WT MICE. The difference in mortality between the 2 mouse strains could potentially reflect differences in ischemic injury after MI induction. However, CMR measurements 1-day post-MI showed that infarct size was similar in WT and *Nlrp3*$^{-/-}$ mice (Figure 1C). The genotypes also had a comparable systolic dysfunction post-MI, as shown by LV ejection fraction (Figure 1D), and LV end-systolic and -diastolic volume as assessed by functional CMR analyses at the same time point (1 day after MI) (Supplemental Figure S3). Together,

these results suggest that the reduced mortality observed in *Nlrp3*$^{-/-}$ mice was not caused by a reduced infarct size or differences in LV function 1 day post-MI.

NLRP3$^{-/-}$ MICE SHOW ATTENUATED LV REMODELING 21 DAYS POST-MI. Acute loss of viable myocardium post-MI results in an abrupt increase in loading conditions that modifies cardiac geometry and function. Activation of inflammatory pathways participates in this process (32). Because female C57BL/6J mice are less prone to myocardial rupture (33), we investigated the remodeling process *in-depth* by subjecting female WT and *Nlrp3*$^{-/-}$ mice to an MI and monitored them for 21 days. A comparable mortality pattern as in male mice was observed, with a higher mortality rate in WT compared with *Nlrp3*$^{-/-}$ mice (43% vs. 12%, respectively; $p < 0.02$), and as in male mice, mice died solely the first week after MI (**Figure 2A**). As expected, however, autopsy revealed that death was mainly due to acute HF, as determined by lung edema and lack of myocardial rupture (10 of 11 WT, 2 of 3 *Nlrp3*$^{-/-}$).

CMR analysis acquired 1, 7, and 21 days post-MI allowed us to carefully assess the infarct healing and remodeling process, revealing again comparable infarct sizes between genotypes at all time points (**Figure 2B**, Supplemental Figure S4). However, in those who survived the first week, only *Nlrp3*$^{-/-}$ mice had some improvement in cardiac function, as implied by a diminished LV dilatation in *Nlrp3*$^{-/-}$ mice, as LV end-diastolic and -systolic volumes, corrected for body weight, increased less over time (−19%; $p < 0.05$ and −25%; $p < 0.05$, respectively) (**Figure 2B**, Supplemental Figure S4).

MEASURES OF CARDIAC FIBROSIS ARE REDUCED IN NLRP3$^{-/-}$ MICE 21 DAYS POST-MI. To further characterize the remodeling process, we measured mRNA expression of selected HF and fibrosis related genes 21 days post-MI. Natriuretic peptide type A (*Nppa*) as marker of ventricular wall stress and IL-6 as marker of inflammation-mediated remodeling were both lower expressed in *Nlrp3*$^{-/-}$ mice in the infarcted LV area (−46%; $p < 0.002$ and −56%; $p < 0.001$, respectively) (**Figure 2C**). Furthermore, markers related to fibrosis (i.e., alpha smooth muscle actin [*Acta2*], matrix metalloproteinase 2 [*Mmp2*], collagen type 1 [*Col1a1*], and collagen type 3 [*Col3a1*]) all had a lower expression in the infarcted LV area in *Nlrp3*$^{-/-}$ mice (−32%; $p < 0.02$; −51%; $p < 0.001$; −35%; $p < 0.02$; −34%; $p < 0.01$, respectively) (**Figure 2C**). Viable LV tissue in *Nlrp3*$^{-/-}$ mice showed decreased expression of *Acta2* and *Mmp2* (−64%; $p < 0.001$; −62%; $p < 0.05$, respectively) (**Figure 2C**). These findings were further supported by the histological evaluation of collagen in the septum area, which was significantly decreased in *Nlrp3*$^{-/-}$ mice (−46%; $p = 0.031$) (**Figure 2D**), all together suggesting attenuated extracellular matrix (ECM) remodeling both within and outside the infarcted area. In contrast, assessment of myocardial tissue did not reveal any differences in cardiomyocyte cross-sectional area between the 2 genotypes (**Figure 2E**). Finally, circulating IL-18 levels were significantly reduced in *Nlrp3*$^{-/-}$ mice 21 days post-MI (−27%; $p < 0.05$) (**Figure 2F**), suggesting persistent down-regulation of NLRP3-derived systemic inflammation in these mice.

MAJOR EFFECTS OF NLRP3 INFLAMMASOME DEFICIENCY ARE ESTABLISHED FIRST DAYS POST-MI. To further understand the process promoting improved infarct healing in *Nlrp3*$^{-/-}$ mice during the first week, we harvested infarcted myocardial tissue from male mice on day 3 and 5 post-MI, reflecting the period of increased mortality in WT mice. The tissue was prepared for quantitative proteomics with the SILAC (stable isotope labelling with amino acids in cell culture) spike in approach. Volcano plots were generated showing that at 3 days post-MI the level of 169 proteins were altered between genotypes; most of them are up-regulated in *Nlrp3*$^{-/-}$ (**Figure 3A**). No significantly expressed proteins were observed at 5 days post-MI, implying that the major effects of NLRP3 inflammasome are during the critical time period prior to the appearance of infarct ruptures. Moreover, annotation enrichment analysis, linking the regulated proteins to pathways and biological processes, found proteins to be enriched in several pathways and biological processes related to tissue repair (**Figure 3B**). Illustrated in **Figure 3C** are significantly regulated proteins involved in regulation of angiogenesis, wound healing, TGFβ receptor signaling pathway, lysosomal transport (GO biological processes), extracellular matrix organization, regulation of insulin-like growth factor (IGF) transport and uptake by IGF binding proteins, integrin cell surface interactions, and platelet degranulation (Reactome gene sets). In general, the protein signature in the *Nlrp3*$^{-/-}$ seems to reflect a more preserved tissue structure and/or an improved tissue repair response. Notably, 1 of the top regulated pathways in the LV tissue, platelet degranulation, has previously been reported as a marker of post-MI pro-resolving macrophages (34), further supporting such a notion.

Due to a large influx of immune cells, especially neutrophils and monocytes/macrophages (35), the first days after MI are often referred to as the inflammatory phase. Three days post-MI decreased

FIGURE 2 ***Nlrp3*** **Deficiency Has a Favorable Effect on Cardiac Remodeling in Mice Up to 21 Days Post-MI**

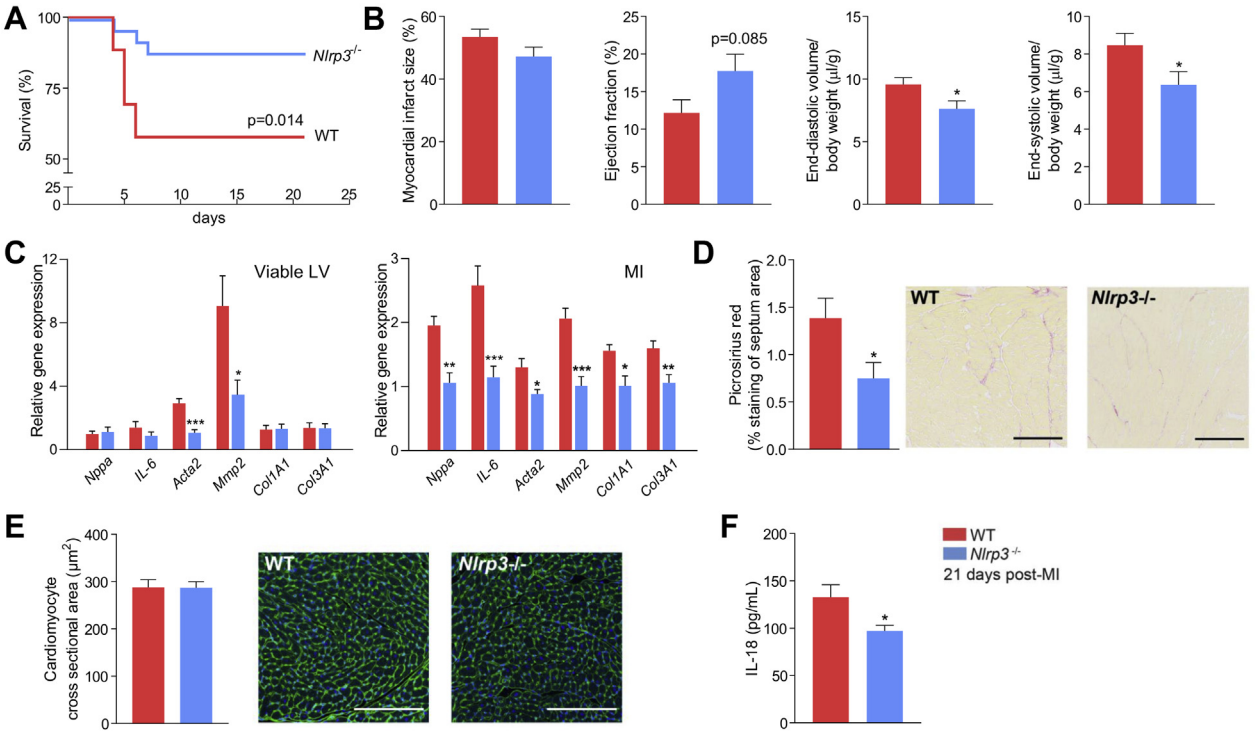

(A) Mortality rates in WT (n = 26) and *Nlrp3*$^{-/-}$ (n = 25) female mice up to 21 days post-MI (p = 0.014, by Kaplan-Meier analysis with log-rank test, 2 independent experiments combined). **(B)** Left ventricular (LV) infarct size, ejection fraction and end-diastolic and -systolic LV volume measured 21 days post-MI by cardiac magnetic resonance (CMR) (n = 7 WT, n = 10 *Nlrp3*$^{-/-}$). **(C)** *Nppa*, *IL-6*, *acta2*, *Mmp2*, *Col1A1*, and *Col3a1* all measured by real-time quantitative polymerase chain reaction, in the viable and infarcted area of LV tissue collected 21 days post-MI in WT (n = 7) and *Nlrp3*$^{-/-}$ (n = 9) mice. **(D)** Collagen percentage, stained with picrosirius red, in interventricular septum in WT (n = 7) and *Nlrp3*$^{-/-}$ (n = 9) mice 21 days post-MI (p = 0.031). Scale bars are 200 µmol/l. **(E)** Cardiomyocyte cross-sectional area, as determined from WGA staining, in the LV in WT (n = 8) and *Nlrp3*$^{-/-}$ (n = 9) mice 21 days post-MI. Scale bars are 200 µmol/l. **(F)** IL-18 levels in plasma measured by enzyme-linked immunosorbent assay 21 days post-MI (p = 0.033; n = 6 mice per genotype). Values are presented as mean ± SEM. *p < 0.05, **p < 0.01, ***p < 0.001. Abbreviations as in Figure 1.

neutrophil numbers were found in *Nlrp3*$^{-/-}$ infarcted area (−63%; p < 0.05) (Supplemental Figure S5), which is consistent with an early effect of NLRP3 deficiency, and improved tissue repair. Macrophage numbers did not differ between the genotypes (Supplemental Figure S5).

HEMATOPOIETIC DEFICIENCY FOR *NLRP3* STRONGLY IMPROVES SURVIVAL AND HEART FUNCTION POST-MI.

Our findings so far point to the early inflammatory phase as the most important temporal window for NLRP3 influence on inadequate tissue healing, maladaptive LV remodeling, development of HF, and mortality. To examine the impact of the infiltrating *Nlrp3*-deficient immune cells in these post-MI processes, we induced MI in WT male mice that had been irradiated and subsequently received WT or *Nlrp3*$^{-/-}$ bone marrow. Nine weeks after bone marrow engraftment (WT to WT 89.4 ± 2.7%; *Nlrp3*$^{-/-}$ to WT 93.5 ± 2.5%) MI was induced and mortality was monitored during a follow-up period of 21 days. This revealed that transplantation of *Nlrp3*$^{-/-}$ bone marrow into WT mice markedly improved post-MI survival compared with WT to WT control subjects (100% vs. 53% survival; p < 0.001) (Figure 4A). As reported before (36), mice did not die during the first week due to rupture, but died primarily during the second week. The main cause of death (8 of 9) was reaching humane endpoints (e.g., reduced body weight and/or severe inactivity). Necropsy revealed that the majority of mice (6 of 9) had lung edema with severely increased lung weight, pointing toward acute HF.

Quantification of infarct size 21 days post-MI demonstrated that infarct size was comparable between groups (Figure 4B). Mean ejection fraction

FIGURE 3 Altered Proteins in *Nlrp3*$^{-/-}$ Mice 3 Days Post-MI Give Differences in Activation Pathways Related to ECM Remodeling

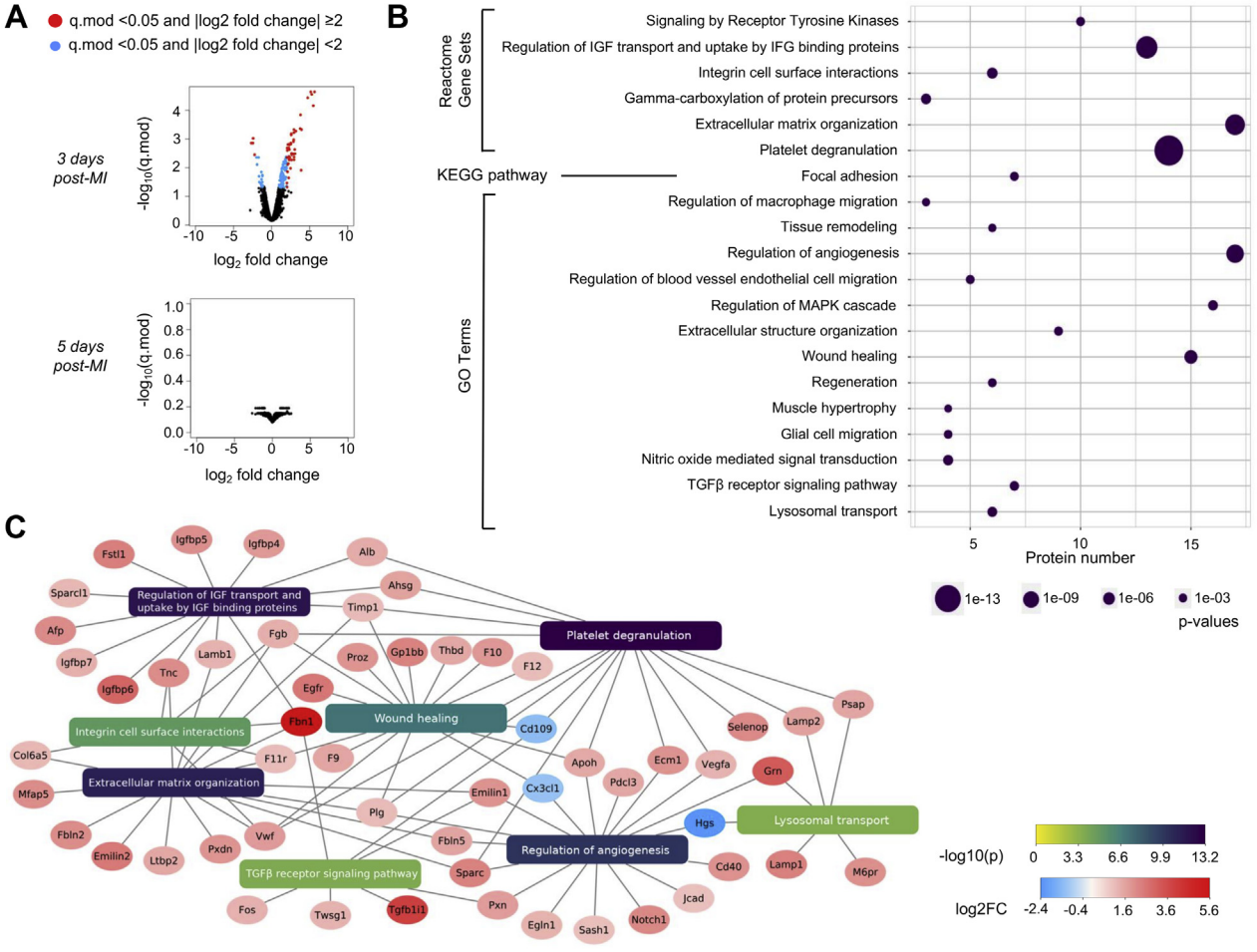

(A) Proteomic abundance from infarcted tissue measured by mass spectrum and compared between WT and *Nlrp3*$^{-/-}$ mice 3 and 5 days post-MI (n = 3 per group). Data illustrated as volcano plots, WT vs. *Nlrp3*$^{-/-}$. **(B)** Enrichment analysis of significantly regulated proteins (moderated q-value <0.05 and $\log_2$Foldchange ≥2), 3 days post-MI. Significantly enriched Reactome pathways, KEGG pathways, and GO Terms are shown. **(C)** Network plot illustrating significantly regulated proteins and their relation to respective Reactome pathways and/or GO processes. The Network plot was created using Cytoscape (28). Abbreviations as in Figure 1. See the Supplemental Material for a list of all abbreviations used that appear in Figure 3. Afp = alpha fetoprotein; Ahsg = alpha-2-HS-glycoprotein; Alb = albumin; Apoh = apolipoprotein H; Cd109 = CD109 antigen; Cd40 = CD40 antigen; Col6a5 = collagen, type VI, alpha 5; Cx3cl1 = chemokine (C-X3-C motif) ligand 1; Ecm1 = extracellular matrix protein 1; Egfr = epidermal growth factor receptor; Egln1 = egl-9 family hypoxia-inducible factor 1; Emilin1 = elastin microfibril interfacer 1; Emilin2 = elastin microfibril interfacer 2; F10 = coagulation factor X; F11r = F11 receptor; F12 = coagulation factor XII (Hageman factor); F9 = coagulation factor IX; Fbln2 = fibulin 2; Fbln5 = fibulin 5; Fbn1 = fibrillin 1; Fgb = fibrinogen beta chain; Fos = FBJ osteosarcoma oncogene; Fstl1 = follistatin-like 1; Gp1bb = glycoprotein Ib, beta polypeptide; Grn = granulin; Hgs = HGF-regulated tyrosine kinase substrate; Igfbp4 = insulin-like growth factor binding protein 4; Igfbp5 = insulin-like growth factor binding protein 5; Igfbp6 = insulin-like growth factor binding protein 6; Igfbp7 = insulin-like growth factor binding protein 7; Lamb1 = laminin B1; Lamp1 = lysosomal-associated membrane protein 1; Lamp2 = lysosomal-associated membrane protein 2; Ltbp2 = latent transforming growth factor beta binding protein 2; M6pr = mannose-6-phosphate receptor, cation dependent; Mfap5 = microfibrillar associated protein 5; Pdcl3 = phosducin-like 3; Plg = plasminogen; Proz = protein Z, vitamin K-dependent plasma glycoprotein; Psap = prosaposin; Pxdn = peroxidasin; Pxn = paxillin; Sash1 = SAM and SH3 domain containing 1; Selenop = selenoprotein P; Sparc = secreted acidic cysteine rich glycoprotein; Sparcl1 = SPARC-like 1; Tgfb1i1 = transforming growth factor beta 1 induced transcript 1; Thbd = thrombomodulin; Timp1 = tissue inhibitor of metalloproteinase 1; Tnc = tenascin C; Twsg1 = twisted gastrulation BMP signaling modulator 1; Vegfa = vascular endothelial growth factor A; Vwf = Von Willebrand factor.

values were 12.9% for WT to WT control subjects vs. 26.3% for *Nlrp3*$^{-/-}$ bone marrow into WT mice ($p = 0.064$) (Figure 4C). Morphometric data, normalized for tibia length, showed increased thickness of the interventricular septum in diastole and systole in WTs receiving bone marrow from *Nlrp3*$^{-/-}$ mice (+85% and +98%, respectively; $p < 0.05$) (Figure 4C), demonstrating less wall thinning (i.e., dilatation) in

FIGURE 4 ***Nlrp3*$^{-/-}$ Bone Marrow Chimeras Have Improved Survival and Less Detrimental Remodeling Post-MI**

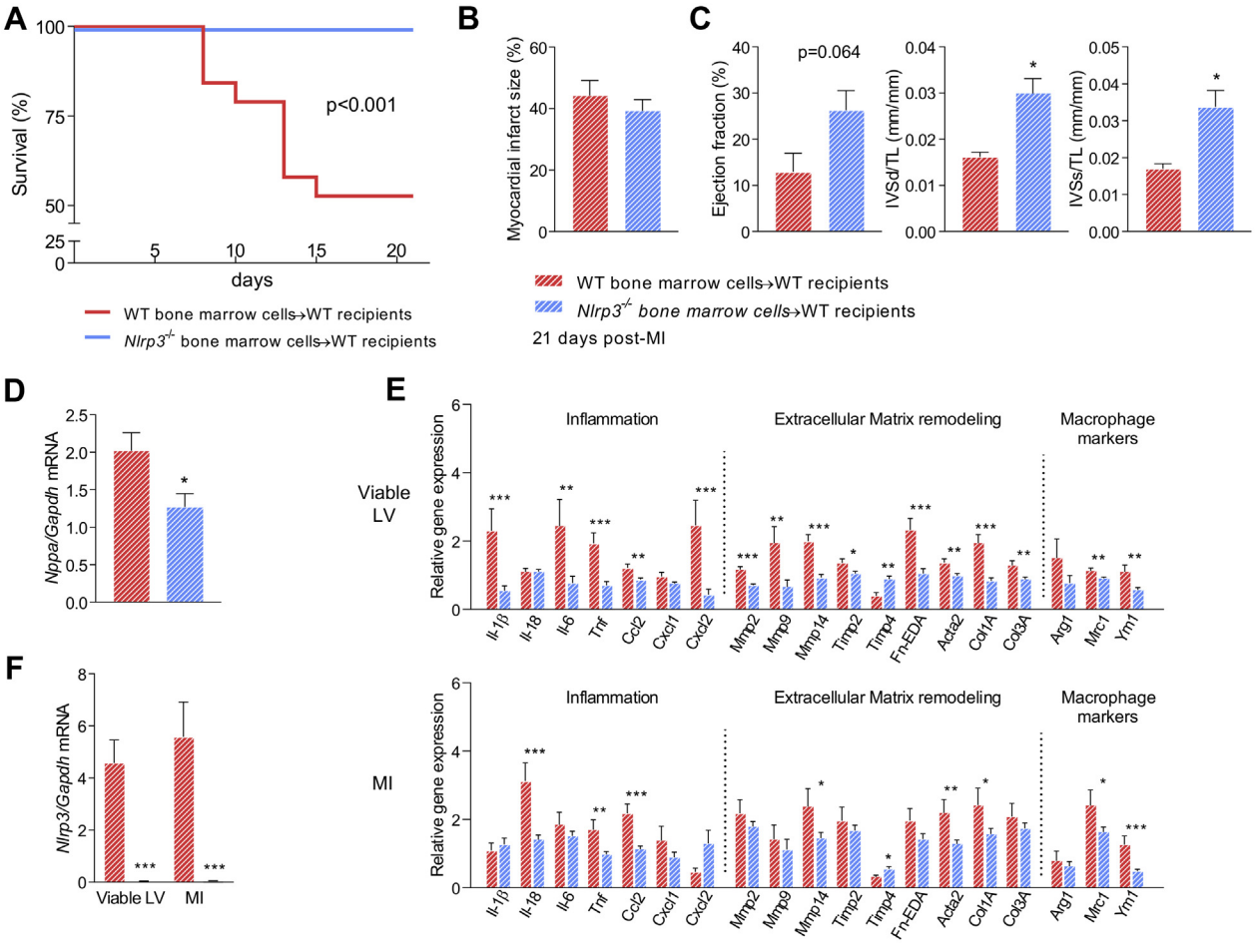

(A) Mortality rates in WT and *Nlrp3*$^{-/-}$ bone marrow chimeric mice up to 21 days after MI ($p < 0.001$, by Kaplan-Meier analysis with log-rank test; n = 19 WT, n = 23 *Nlrp3*$^{-/-}$). **(B)** Left ventricle (LV) infarct size measured by picrosirius red staining (n = 9 WT, n = 22 *Nlrp3*$^{-/-}$) and **(C)** ejection fraction and interventricular septum (IVS) thickness in diastole (d) and systole (s) adjusted for tibia length (TL) measured 21 days post-MI by echocardiography (n = 9 WT, n = 23 *Nlrp3*$^{-/-}$). **(D)** LV tissue *Nppa* mRNA levels measured by real-time quantitative polymerase chain reaction. **(E)** mRNA levels of several genes measured by real-time quantitative polymerase chain reaction, in the viable and infarcted LV tissue collected 21 days post-MI in chimera mice (n = 9 WT, n = 23 *Nlrp3*$^{-/-}$). **(F)** *Nlrp3*$^{-/-}$ mRNA levels in viable and infarcted LV tissue 21 days post-MI in chimera mice (n = 9 WT, n = 23 *Nlrp3*$^{-/-}$). Values are presented as mean ± SEM. *$p < 0.05$, **$p < 0.01$, ***$p < 0.001$. Abbreviations as in Figure 1.

WT mice who received bone marrow from *Nlrp3*$^{-/-}$ mice. In line with this, WT mice receiving bone marrow from *Nlrp3*$^{-/-}$ mice had decreased expression of *Nppa* (−37%; $p < 0.05$) in viable LV (Figure 4D). Further characterization of gene regulation in the viable and infarcted LV tissue of these mice supported a less detrimental tissue remodeling with regulated genes related to inflammation, ECM remodeling, and macrophage polarization (Figure 4E).

CARDIAC EXPRESSION OF NLRP3 IN THE CHRONIC PHASE AFTER MYOCARDIAL INFARCTION IS RESTRICTED TO HEMATOPOIETIC CELLS. We also investigated if NLRP3 was expressed in the infarcted area 21 days post-MI in WT mice transplanted with WT or *Nlrp3*$^{-/-}$ bone marrow. Strikingly, in contrast to WT mice that had received WT bone marrow, no expression of *Nlrp3* was found in the infarcted area or in viable LV of WT mice with *Nlrp3*$^{-/-}$ bone marrow ($p < 0.0001$) (Figure 4F), strongly supporting that

FIGURE 5 ***Nlrp3*$^{-/-}$ Peritoneal Macrophage Have Improved Clearance of Apoptotic Cells**

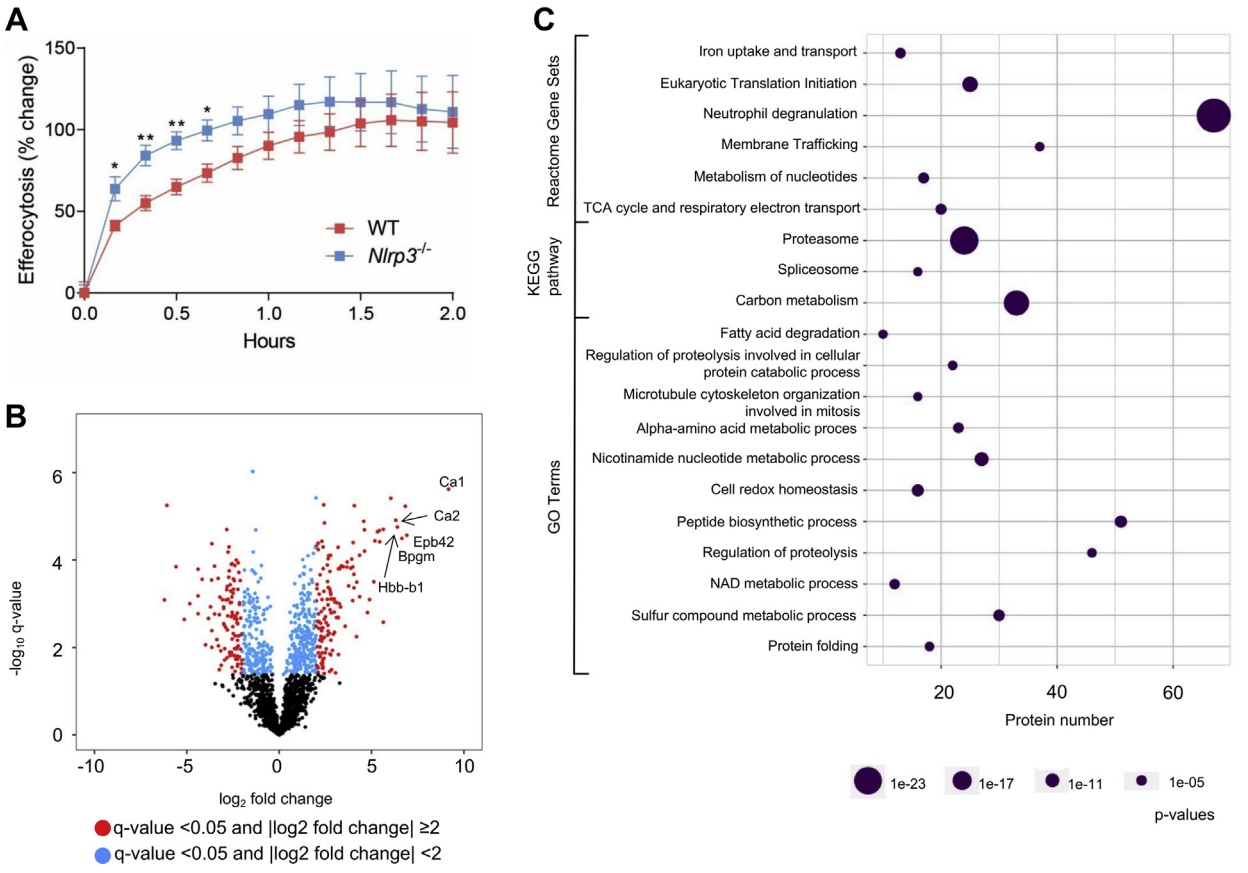

(A) Peritoneal macrophages from WT and *Nlrp3*$^{-/-}$ mice were coincubated with pHrodo-labeled apoptotic Jurkat T cells and efferocytosis was monitored for 2 h. (n = 6 per genotype). Data is presented as mean ± SEM. *p < 0.05, **p < 0.01. **(B)** Protein expression in peritoneal macrophages from WT vs. *Nlrp3*$^{-/-}$ mice illustrated by a volcano plot. Erythrocyte proteins are named in the Figure. **(C)** Enrichment analysis of significantly regulated proteins (q-value < 0.05 and $\log_2$Foldchange ≥1), 3 days post-MI. Significantly enriched Reactome pathways, KEGG pathways, and GO Terms are shown. Bpgm = Bisphosphoglycerate Mutase; Ca1 = carbonic anhydrase 1; Ca2 = carbonic anhydrase 2; Epb42 = Erythrocyte Membrane Protein Band 4.2; Hbb-b1 = Hemoglobin subunit beta-1.

cardiac *Nlrp3* expression, at this time point, is confined to hematopoietic cells.

ENHANCED EFFEROCYTOTIC CAPACITY OF MACROPHAGES IN *NLRP3*$^{-/-}$ MICE. One of the main tasks of the infiltrating immune cells during the early inflammatory phase is clearance of dead cells and debris, thereby facilitating cardiac repair (34,37). Macrophages play a major role in this process, and we therefore evaluated the scavenging capacity of *Nlrp3*$^{-/-}$ macrophages.

Peritoneal macrophages were challenged in vitro with apoptotic Jurkat T cells, and the efferocytotic capacity was measured over time. *Nlrp3*$^{-/-}$ macrophages displayed an increased efferocytic velocity (i.e., engulfment of apoptotic cells), supporting a pro-resolving phenotype of *Nlrp3*$^{-/-}$ macrophages (Figure 5A). Then, to investigate the phenotype further, unstimulated WT and *Nlrp3*$^{-/-}$ macrophages were isolated for label-free quantitative proteomics analysis. The isolated *Nlrp3*$^{-/-}$ macrophages had a distinct red color, even after several washing procedures (data not shown). Interestingly, the most regulated proteins found in the proteomics analysis were proteins found in erythrocytes, strongly suggesting that the observed red color was due to increased erythrocyte efferocytosis among the *Nlrp3*$^{-/-}$ macrophages (Figure 5B). In line with this, *Nlrp3*$^{-/-}$ macrophages had increased levels of the phagocytic marker CD36 and Prdx2 (34) (q > 0.05, log2FC 2.3 and 4.6, respectively). Enrichment analysis indicated altered

metabolic phenotype in the *Nlrp3*$^{-/-}$ macrophages with regulated membrane trafficking (Reactome, 37/564 proteins), regulation of proteolysis (GO, 45/729 proteins) and increased proteasomal activity (Proteasome KEGG pathway, 24/46 proteins, all up-regulated) (Figure 5C). In summary, these data show that the *Nlrp3*$^{-/-}$ macrophages are more active with an improved apoptotic cell clearance capacity.

DISCUSSION

THE NLRP3 INFLAMMASOME EXACERBATE INFARCT REPAIR AND REMODELING. In the present study, we show that *Nlrp3* deficiency improves post-MI survival in the short-term (i.e., after 7 days) and counteracts long-term (i.e., 21 days) maladaptive myocardial remodeling. Proteome analysis 3 days post-MI revealed an early beneficial effect of NLRP3 deficiency, with regulated pathways and processes related to wound healing, ECM organization, and angiogenesis. Notably, these changes were accompanied by decreased amounts of neutrophils within the infarcted area of *Nlrp3*$^{-/-}$ mice. The importance of immune cells for the beneficial phenotype of the *Nlrp3*$^{-/-}$ mice was demonstrated by the recapitulation of the *Nlrp3*$^{-/-}$ phenotype in WT mice transplanted with *Nlrp3*$^{-/-}$ bone marrow. Finally, in vitro data showed that *Nlrp3*$^{-/-}$ macrophages have a pro-resolving phenotype (i.e., enhanced efferocytosis), suggesting improved clearance of apoptotic cells and cellular debris as an important component that could explain the favorable myocardial repair response in *Nlrp3*$^{-/-}$. Our findings suggest that targeting NLRP3-mediated inflammation could be an attractive therapeutic approach, not only in atherosclerotic disorders (6), but also during MI to reduce acute and chronic complications following this event.

NONREPERFUSED MI MODEL. There are several experimental studies on the role of NLRP3 inflammasome during MI, but most of these are focusing on its role in I/R, showing different responses at least partly depending on the models employed (7–10). In the present study, we used a non-reperfused MI model, showing detrimental effects of NLRP3 on early infarct healing, as demonstrated by reduced mortality, mostly caused by myocardial rupture, during the first week in *Nlrp3*$^{-/-}$ mice. Death by myocardial rupture is no longer a common problem in the clinic due to supportive medical treatment. However, in the experimental setting, myocardial rupture may still be of explanatory value as it reflects attenuated tissue repair, which is an important issue also in clinical medicine.

NLRP3 INFLAMMASOME INFLUENCES LONG-TERM REMODELING. Although there are some studies on the short-time effect of NLRP3 deficiency following MI, data on the effect on long-term myocardial remodeling are limited (38). Despite the possible selection bias of the healthier WT mice due to early mortality of the sickest animals, we still detected in the present study a beneficial effect on myocardial remodeling at 21 days in the surviving *Nlrp3*$^{-/-}$ mice. Because the regenerative capacity of the heart is nearly absent, dead tissue is replaced by a collagen rich scar, which lacks contractile function. Notably, proteomic analyses of the infarcted tissue at 3 days, but not at 5 days, post-MI suggested a more favorable tissue repair in *Nlrp3*$^{-/-}$ mice with significantly regulated proteins enriched in processes like wound healing, ECM organization, TGFB signaling, and angiogenesis. Later, 21 days after MI, NLRP3-deficient mice showed less fibrosis and reduced level of pro-fibrotic genes (i.e., *Acta2*, *Mmp2*, and *IL-6*) compared with WT. A more favorable tissue remodeling was also found in WT animals receiving *Nlrp3*$^{-/-}$ bone marrow. Thus, the improved tissue healing in *Nlrp3*$^{-/-}$ infarcted hearts the first days after MI may also lead to less adverse ECM remodeling later, leading to preserved cardiac function.

THE NLRP3-DEFICIENT MACROPHAGE. Macrophages are important cells for orchestrating ECM modulation in tissue repair and remodeling after MI (39). Efficient clearance of apoptotic cells (efferocytosis) is a prerequisite for resolution of inflammation and tissue repair following MI (40). In the present study, we provide several lines of evidence suggesting that the lack of NLRP3 changes the macrophage toward a more phagocytosing and resolving phenotype. First, we showed increased efferocytotic velocity in peritoneal macrophages from NLRP3-deficient cells. Second, we demonstrated increased in vivo erythrocyte clearance in peritoneal macrophages from *Nlrp3*$^{-/-}$ mice. Third, in the proteomics data, we find regulation of metabolic activity and especially proteasome activity, together with up-regulation of the phagocytosis markers, CD36 and Prdx2 (34) further supporting macrophage activity related to removal cell debris and apoptotic cells (i.e., resolving activity). Fourth, within the LV, NLRP3-

deficient mice showed enhanced activation of pathways related to lysosomal transport, at least in some degree supporting such activity also within the myocardium. Finally, the top-regulated pathways in the LV tissue, platelet degranulation, also including proteins involved in regulation of proteolysis, has previously been reported as a marker of post-MI pro-resolving macrophages (34) These data indicate that macrophages of NLRP3-deficient mice have enhanced activity of processes related to removal of apoptotic cells and cell debris, and this seems also to operate within the myocardium. Thus, it is tempting to speculate that a *Nlrp3*$^{-/-}$ macrophage, with its resolving phenotype, accelerates the repair process, improving tissue healing. This may be an explanation for the improved infarct healing observed in the *Nlrp3*$^{-/-}$ mice in this study, and the ultimate reason for the improved myocardial remodeling and function observed in the *Nlrp3*$^{-/-}$ mice at day 21. Thus, although there were no differences in infarct size between the 2 genotypes, the quality of the infarcted area seems to be improved in *Nlrp3*$^{-/-}$ mice possibly involving a pro-resolving macrophage phenotype in these mice. Moreover, as we found no difference in macrophage infiltration within the myocardium between the 2 genotypes, this seems not to merely reflect altered numbers of these cells.

LEUKOCYTES AND NLRP3 INFLAMMASOMES. The localization of NLRP3 inflammasomes within the heart is still somewhat unclear. In the present study, we suggest that NLRP3 inflammasome within the post-MI myocardium mainly originates from hematopoietic cells. First, we showed that the beneficial effects of *Nlrp3* deficiency on mortality and myocardial remodeling following MI were also observed in WT mice that received bone marrow from *Nlrp3*$^{-/-}$ mice. Moreover, no expression of *Nlrp3* was found in the LV of WT mice that had received bone marrow from *Nlrp3*$^{-/-}$ mice, indicating that cardiac *Nlrp3* expression, at least at this time point, is confined to hematopoietic cells. Protti et al. (36) reported that after a bone marrow transplant (*before* MI), 92% of the host cardiac macrophage population was replaced by donor cells. Therefore, both resident and infiltrating *Nlrp3*-deficient immune cells may have been contributing to the beneficial remodeling process after bone marrow transplantation. All together, these results demonstrate the importance of immune cells in mediating the harmful effects of NLRP3 inflammasome during MI. As we, by our experimental set-up, only could measure *Nlrp3* expression at a late time-point post-MI, other nonleukocytes may still have been expressing *Nlrp3* earlier in the repair process. Future studies should therefore look into the early interactions between infiltrating immune cells, resident immune cells, and other cardiac cells that also have been shown to express NLRP3 (cardiac fibroblasts [41], endothelial cells [42], and cardiomyocytes [41,43,44]) in post-MI cardiac tissue.

CLINICAL RELEVANCE. Our study demonstrates the potential of NLRP3 inflammasome inhibition in MI. Whereas the CANTOS trial showed a beneficial role for IL-1β inhibition on cardiovascular events in patients with atherosclerosis and previous MI (45), so far clinical trials on specific NLRP3 inflammasome inhibition during acute MI are nearly lacking. However, blocking IL-1 by IL-1 receptor antagonist anakinra has been shown to down-regulate inflammation during MI (46), and a larger multicenter study on the effect of anakinra in patients with MI is currently ongoing (47).

Previous studies have found that neutralization of IL-1β or -18 in experimental MI give findings that are comparable to what we present in the current study, that is, no reduction in infarct size, but improved cardiac remodeling (48–50). However, the effect of inhibiting NLRP3 could extend beyond that of reducing generation of active IL-1β and -18. Although IL-1β and -18 are the most studied caspase-1 substrates, there are many other verified and potential substrates that could be important during myocardial infarction (51). NLRP3-dependent caspase-1 activation can, through cleavage of gasdermin D, induce programmed necrosis (i.e., pyroptosis) and promote an inflammatory response that is IL-1 and -18 independent (52). NLRP3 may also regulate functions such as phagosome formation and cellular metabolism, and of particular relevance to findings in this paper, eicosanoid production (53,54). The role of NLRP3 in increasing macrophage production of inflammatory lipid mediators, independently of IL-1β and -18, represents a mechanism that inhibits physiological resolution of inflammation and could very well at least partly explain our findings on efferocytosis in Nlrp3-deficient macrophages.

Finally, we emphasize that a direct comparison of NLRP3 inhibition and neutralization of IL-1β and -18 in a setting of post-myocardial infarction remodeling is a natural and important extension of our and others' findings. Such studies are necessary to identify both similarities and differences regarding effects on pathogenic mechanisms and, most importantly, therapeutic efficacy and safety.

STUDY LIMITATIONS. First, the model we chose for our experiments, nonreperfused MI, could be regarded less clinically relevant as the myocardial tissue is not reperfused as in a clinical setting. As we, by this model, may study effects that are less dependent on initial infarct size and reperfusion damage, we still find the method valuable. Second, due to housing limitations, we have performed homozygous breeding. The animals used are housed together, but are thus not littermates. Third, whereas the main studies consist of a large number of mice, the substudies have a smaller sample size. Fourth, we have not used male and female mice for all studies, but focused mainly on male mice except for the remodeling study. Fifth, due to the bone marrow transplantation study set-up, we lack data on early time points to investigate recruitment and clearance of cells. Sixth, the phenotypic characterization of mainly neutrophils and to lesser extent macrophages is partially lacking. Finally, we lack direct evidence of data on macrophage removal of apoptotic cells within the myocardium.

CONCLUSIONS

We show that NLRP3 deficiency attenuates mortality, maladaptive remodeling, and development of HF following MI. We suggest that macrophages showing enhanced efferocytosis capacity in *Nlrp3*$^{-/-}$ mice may play a key role in the beneficial phenotype in these mice. The role of infiltrating immune cells was strongly supported by our bone marrow transplant experiment, recapitulating the *Nlrp3*$^{-/-}$ phenotype in WT mice that had been transplanted with *Nlrp3*$^{-/-}$ bone marrow. Our data should encourage performing clinical trials directly inhibiting NLRP3 inflammasome and its target inflammatory cytokines (IL-1β and -18) in MI patients.

ACKNOWLEDGMENTS The authors thank Solveig B. Haugstad, Emil K.S. Espe, and Kenneth Schneider for their excellent technical assistance in relation to CMR measurements.

AUTHOR DISCLOSURES

This work was supported by grants from the K.G. Jebsen Inflammation Research Centre, South-Eastern Norway Regional Health Authority, and Norwegian Research Council. Dr. Yndestad is currently an employee of Pfizer Norway; the current work was conducted when he was employed by Oslo University Hospital. All other authors have reported that they have no relationships relevant to the contents of this paper to disclose.

ADDRESS FOR CORRESPONDENCE: Dr. Pål Aukrust, Oslo University Hospital, Rikshospitalet, Postboks 4950 Nydalen, 0424 Oslo, Norway. E-mail: paukrust@ous-hf.no.

PERSPECTIVES

COMPETENCY IN MEDICAL KNOWLEDGE: An excessive or prolonged inflammatory response after MI may disturb formation of a stable scar and promote adverse LV remodeling, leading to impaired myocardial function and heart failure.

TRANSLATIONAL OUTLOOK: Our results highlight the detrimental role of the NLRP3 inflammasome and infiltrating immune cells in the subacute phase after MI. Further studies that directly compare NLRP3 inhibition and neutralization of IL-1β and -18 in this setting are natural and important extensions of our and others' findings and could encourage clinical trials.

REFERENCES

1. Frangogiannis NG, Smith CW, Entman ML. The inflammatory response in myocardial infarction. Cardiovasc Res 2002;53:31–47.

2. Mann DL. The emerging role of innate immunity in the heart and vascular system: for whom the cell tolls. Circ Res 2011;108:1133–45.

3. Epelman S, Liu PP, Mann DL. Role of innate and adaptive immune mechanisms in cardiac injury and repair. Nat Rev Immunol 2015;15:117–29.

4. Bryan NB, Dorfleutner A, Rojanasakul Y, Stehlik C. Activation of inflammasomes requires intracellular redistribution of the apoptotic speck-like protein containing a caspase recruitment domain. J Immunol 2009;182:3173–82.

5. Dinarello CA. A clinical perspective of IL-1beta as the gatekeeper of inflammation. Eur J Immunol 2011;41:1203–17.

6. Baldrighi M, Mallat Z, Li X. NLRP3 inflammasome pathways in atherosclerosis. Atherosclerosis 2017;267:127–38.

7. Toldo S, Marchetti C, Mauro AG, et al. Inhibition of the NLRP3 inflammasome limits the inflammatory injury following myocardial ischemia-reperfusion in the mouse. Int J Cardiol 2016;209:215–20.

8. Sandanger O, Gao E, Ranheim T, et al. NLRP3 inflammasome activation during myocardial ischemia reperfusion is cardioprotective. Biochem Biophys Res Commun 2016;469:1012–20.

9. Kawaguchi M, Takahashi M, Hata T, et al. Inflammasome activation of cardiac fibroblasts is essential for myocardial ischemia/reperfusion injury. Circulation 2011;123:594–604.

10. Jong WM, Leemans JC, Weber NC, et al. Nlrp3 plays no role in acute cardiac infarction due to low cardiac expression. Int J Cardiol 2014;177:41–3.

11. Mezzaroma E, Toldo S, Farkas D, et al. The inflammasome promotes adverse cardiac remodeling following acute myocardial infarction in the mouse. Proceedings of the Proc Natl Acad Sci U S A 2011;108:19725–30.

12. van Hout GP, Bosch L, Ellenbroek GH, et al. The selective NLRP3-inflammasome inhibitor MCC950 reduces infarct size and preserves cardiac

function in a pig model of myocardial infarction. Eur Heart J 2017;38:828–36.

13. Kanneganti TD, Ozoren N, Body-Malapel M, et al. Bacterial RNA and small antiviral compounds activate caspase-1 through cryopyrin/Nalp3. Nature 2006;440:233–6.

14. Ozoren N, Masumoto J, Franchi L, et al. Distinct roles of TLR2 and the adaptor ASC in IL-1beta/IL-18 secretion in response to Listeria monocytogenes. J Immunol 2006;176:4337–42.

15. Gao E, Lei YH, Shang X, et al. A novel and efficient model of coronary artery ligation and myocardial infarction in the mouse. Circ Res 2010;107:1445–53.

16. Schindelin J, Arganda-Carreras I, Frise E, et al. Fiji: an open-source platform for biological-image analysis. Nat Methods 2012;9:676–82.

17. Konzer A, Ruhs A, Braun T, Krüger M. Global protein quantification of mouse heart tissue based on the SILAC mouse. In: Vivanco F, editor. Heart Proteomics: Methods and Protocols. Totowa, NJ: Humana Press, 2013:39–52.

18. Kammers K, Cole RN, Tiengwe C, Ruczinski I. Detecting significant changes in protein abundance. EuPA Open Proteom 2015;7:11–9.

19. Smyth GK. Linear models and empirical bayes methods for assessing differential expression in microarray experiments. Stat Appl Genet Mol Biol 2004;3:16646809.

20. Zhou Y, Zhou B, Pache L, et al. Metascape provides a biologist-oriented resource for the analysis of systems-level datasets. Nat Commun 2019;10:1523.

21. The Gene Ontology Resource: 20 years and still GOing strong. Nucleic Acids Res 2019;47:D330–8.

22. Ashburner M, Ball CA, Blake JA, et al. Gene ontology: tool for the unification of biology. The Gene Ontology Consortium. Nat Gen 2000;25:25–9.

23. Jassal B, Matthews L, Viteri G, et al. The reactome pathway knowledgebase. Nucleic Acids Res 2020;48:D498–503.

24. Kanehisa M. Toward understanding the origin and evolution of cellular organisms. Protein Sci 2019;28:1947–51.

25. Kanehisa M, Goto S. KEGG: kyoto encyclopedia of genes and genomes. Nucleic Acids Res 2000;28:27–30.

26. Kanehisa M, Sato Y, Furumichi M, Morishima K, Tanabe M. New approach for understanding genome variations in KEGG. Nucleic Acids Res 2019;47:D590–5.

27. Wickham H. ggplot2: Elegant Graphics for Data Analysis. New York: Springer-Verlag, 2016.

28. Shannon P, Markiel A, Ozier O, et al. Cytoscape: a software environment for integrated models of biomolecular interaction networks. Genome Res 2003;13:2498–504.

29. Tyanova S, Temu T, Cox J. The MaxQuant computational platform for mass spectrometry-based shotgun proteomics. Nat Protoc 2016;11:2301–19.

30. Tyanova S, Temu T, Sinitcyn P, et al. The Perseus computational platform for comprehensive analysis of (prote)omics data. Nat Methods 2016;13:731–40.

31. Blighe K, Rana S, Lewis M. EnhancedVolcano: Publication-ready volcano plots with enhanced colouring and labeling. R package version 1.6.0 edition; 2020.

32. Frangogiannis NG. The inflammatory response in myocardial injury, repair, and remodelling. Nat Rev Cardiol 2014;11:255–65.

33. Gao XM, Xu Q, Kiriazis H, Dart AM, Du XJ. Mouse model of post-infarct ventricular rupture: time course, strain- and gender-dependency, tensile strength, and histopathology. Cardiovasc Res 2005;65:469–77.

34. Mouton AJ, DeLeon-Pennell KY, Rivera Gonzalez OJ, et al. Mapping macrophage polarization over the myocardial infarction time continuum. Basic Res Cardiol 2018;113:26.

35. Frangogiannis NG. Regulation of the inflammatory response in cardiac repair. Circ Res 2012;110:159–73.

36. Protti A, Mongue-Din H, Mylonas KJ, et al. Bone marrow transplantation modulates tissue macrophage phenotype and enhances cardiac recovery after subsequent acute myocardial infarction. J Mol Cell Cardiol 2016;90:120–8.

37. van Amerongen MJ, Harmsen MC, van Rooijen N, Petersen AH, van Luyn MJ. Macrophage depletion impairs wound healing and increases left ventricular remodeling after myocardial injury in mice. Am J Pathol 2007;170:818–29.

38. Gao R, Shi H, Chang S, et al. The selective NLRP3-inflammasome inhibitor MCC950 reduces myocardial fibrosis and improves cardiac remodeling in a mouse model of myocardial infarction. Int Immunopharmacol 2019;74:105575.

39. O'Rourke SA, Dunne A, Monaghan MG. The role of macrophages in the infarcted myocardium: orchestrators of ECM remodeling. Front Cardiovasc Med 2019;6:101.

40. Serhan CN, Savill J. Resolution of inflammation: the beginning programs the end. Nat Immunol 2005;6:1191–7.

41. Bracey NA, Beck PL, Muruve DA, et al. The Nlrp3 inflammasome promotes myocardial dysfunction in structural cardiomyopathy through interleukin-1β. Exp Physiol 2013;98:462–72.

42. Liu Y, Lian K, Zhang L, et al. TXNIP mediates NLRP3 inflammasome activation in cardiac microvascular endothelial cells as a novel mechanism in myocardial ischemia/reperfusion injury. Basic Res Cardiol 2014;109:415.

43. Sandanger Ø, Ranheim T, Vinge LE, et al. The NLRP3 inflammasome is up-regulated in cardiac fibroblasts and mediates myocardial ischaemia-reperfusion injury. Cardiovasc Res 2013;99:164–74.

44. Suetomi T, Willeford A, Brand CS, et al. Inflammation and NLRP3 inflammasome activation initiated in response to pressure overload by ca(2+)/calmodulin-dependent protein kinase II δ signaling in cardiomyocytes are essential for adverse cardiac remodeling. Circulation 2018;138:2530–44.

45. Ridker PM, Everett BM, Thuren T, et al. Antiinflammatory therapy with canakinumab for atherosclerotic disease. N Engl J Med 2017;377:1119–31.

46. Morton AC, Rothman AM, Greenwood JP, et al. The effect of interleukin-1 receptor antagonist therapy on markers of inflammation in non-ST elevation acute coronary syndromes: the MRC-ILA Heart Study. Eur Heart J 2015;36:377–84.

47. Van Tassell BW, Lipinski MJ, Appleton D, et al. Rationale and design of the Virginia Commonwealth University-Anakinra Remodeling Trial-3 (VCU-ART3): a randomized, placebo-controlled, double-blinded, multicenter study. Clin Cardiol 2018;41:1004–8.

48. Abbate A, Van Tassell BW, Seropian IM, et al. Interleukin-1beta modulation using a genetically engineered antibody prevents adverse cardiac remodelling following acute myocardial infarction in the mouse. Eur J Heart Fail 2010;12:319–22.

49. Toldo S, Mezzaroma E, Van Tassell BW, et al. Interleukin-1β blockade improves cardiac remodelling after myocardial infarction without interrupting the inflammasome in the mouse. Exp Physiol 2013;98:734–45.

50. Wang M, Tan J, Wang Y, Meldrum KK, Dinarello CA, Meldrum DR. IL-18 binding protein-expressing mesenchymal stem cells improve myocardial protection after ischemia or infarction. Proc Natl Acad Sci U S A 2009;106:17499–504.

51. Denes A, Lopez-Castejon G, Brough D. Caspase-1: is IL-1 just the tip of the ICEberg? Cell Death Dis 2012;3:e338.

52. Bergsbaken T, Fink SL, Cookson BT. Pyroptosis: host cell death and inflammation. Nat Rev Microbiol 2009;7:99–109.

53. Lee S, Nakahira K, Dalli J, et al. NLRP3 Inflammasome deficiency protects against microbial sepsis via increased lipoxin B(4) synthesis. Am J Respir Crit Care Med 2017;196:713–26.

54. Rathinam VA, Fitzgerald KA. Inflammasome complexes: emerging mechanisms and effector functions. Cell 2016;165:792–800.

KEY WORDS cardiac remodeling, hematopoietic cells, innate immunity, macrophages, myocardial infarction, NLRP3

APPENDIX For supplemental figures, please see the online version of this paper.